Segmentation Effects in the Modular HVDC Offshore Wind Generator and its Impact on Losses

1st Yannick Cyiza Karekezi
Dep. of electric power engineering
NTNU
Trondheim, Norway
Yannick.c.karekezi@ntnu.no

2nd Zhaoqiang Zhang
Dep. of electric power engineering
NTNU
Trondheim, Norway
zhaoqiang.zhang@ntnu.no

3rd Pål Keim Olsen
Dep. of electric power engineering
NTNU
Trondheim, Norway
pal.keim.olsen@ntnu.no

2023 IEEE 32nd International Symposium on Industrial Electronics (ISIE) | 979-8-3503-9971-4/23/$31.00 ©2023 IEEE | DOI: 10.1109/ISIE51358.2023.10227955

***Abstract*—Worldwide wind power capacity jumped from $7.5\,\mathrm{GW}$ in 1997 to $564\,\mathrm{GW}$ by 2018, according to IRENA. Many regions of the world have strong wind speeds, but the best locations for generating wind power are often remote, where offshore wind power offers tremendous potential. This paper presents a concept to remove the use of offshore platforms/substations, constituting the energy conditioning element for the high voltage direct current (HVDC) transmission. Instead, it connects converters in a series of modules for a segmented HVDC generator, which limits the number of conversion steps. Our work focuses on the impact of segmentation on loss and is validated numerically using finite element analysis (FEA) and analytical solutions. The machine's geometry, design constraints, design procedure, loss calculations, and numerical analysis are included. Three different methods are presented and used to determine the core losses. The paper highlights the increase in core losses due to airgap segmentation. We show that Zhang's method yield the largest deviation in the loss calculations, i.e., $15.812\,\%$, $16.410\,\%$ and $15.894\,\%$ increase in core losses for 10, 20 and $30\,\mathrm{mm}$ segment airgaps, respectively.**

***Index Terms*—Synchronous machines, machine design, Finite Element Analysis (FEA), numerical simulation, voltage simulation.**

NOMENCLATURE

α	Relative pole width, $[pu]$
δ_{min}	Minimum airgap, $[mm]$
η	Generator efficiency, $[\%]$
ω_e	Electrical speed, $[\mathrm{rad/s}]$
τ_u, τ_p	Slot and pole pitch, $[\mathrm{mm}]$
Θ_q	Load angle, $[\mathrm{rad}]$
φ	Power factor, [–]
A_{cus}	Stator bar cross section, $[\mathrm{m}^2]$
A_s	Armature loading, [pu] or $[\mathrm{A}^2/\mathrm{mm}^2/\mathrm{cm}]$
B_δ, B_{pk}	Airgap and pole body flux density, [T]
B_{sy}, B_{ry}	Stator and rotor yoke flux density, [T]
B_{th}	Stator teeth flux density, [T]
D_o, D_i	Outer and inner stator diameter, $[\mathrm{mm}]$
D_{ro}, D_{ri}	Outer and inner rotor diameter, $[mm]$
f	Nominal electrical frequency, [Hz]
F_d	Tangential force density, $[\mathrm{kN/m}^2]$
h_{cus}, b_{cus}	Height and width of strand, $[\mathrm{mm}]$
h_s, w_{st}, w_{tt}	Slot height,width and tooth width, $[mm]$
I_a, $\hat{I}$	Rated stator armature current RMS and peak fundamental, [pu] or [A]
i_a, i_b, i_c	stator instantaneous currents, [pu] or [A]
J_s	Stator winding current density, $[\mathrm{A/mm}^2]$
l_b	Gross iron length, $[\mathrm{m}]$
n	Rated mechanical speed, $[\mathrm{rpm}]$
N_s	Turns per coil, [–]
P_{cu}, P_s, P_{fe}	Stator winding, stray load, and iron core loss, [pu] or [kW]
P_{nom}	Nominal power, [pu] or [MW]
P_{pm}	Permanent magnet losses, [pu] or $[kW]$
q, w_w, k_w,	Slots per pole and phase, coil span, and winding factor, [–]
S, S_b	Apparent and base apparent generator power, [pu] or [MVA]
t_{ins}	Insulation thickness, $[mm]$
U_a, $\mathcal{E}_g$	Armature and induced voltage, [pu] or [V]
w_{seg}	Segment airgap length, $[mm]$

I. INTRODUCTION

In this paper, the concept of a modular HVDC generator [1] is presented. The paper also presents a way to remove the use of offshore platforms/substations, which constitute the energy conditioning element for the HVDC transmission, and instead connect converters in a series of modules for a segmented HVDC generator [2]. The generating units of typical wind energy conversion systems consist of several components: wind turbines, generators, electronic converters, and transformers, which condition the energy produced, in addition to other parts [3]. Due to its nature, grid connection is especially challenging for offshore applications [4]. With the current wind farm configuration, it is still necessary to use transformers, AC/DC, and DC/DC converters for HVDC transmission [5], which is required to condition the AC power at the output of the generators into DC power with a high voltage value. The method used to interconnect the different components to the electric grid plays a fundamental role in reducing cost and improving the efficiency, reliability, and performance of wind farms [6]. The number of conversion steps is significantly reduced because HVDC is reached in the first conversion step [7]–[10], which could reduce the wind farm's costs, efficiency, and reliability [11]. The paper is divided into four sections.

1) Introduction;

TABLE I
RATED MACHINE SPECIFICATION FOR GENERATOR G1

P_{nom}	n	f	U_a
15 MW	10 rpm	26.67 Hz	80 kV

TABLE II
DESIGN CONSTRAINTS FOR GENERATOR G1

J_s	B_t	B_{ry}	B_{sy}
≤3.0 $\mathrm{A/mm^2}$	≤1.80 T	≤1.50 T	≤1.50 T

TABLE III
DESIGN CRITERIA FOR GENERATOR G1

$A_s = K_c \cdot J_c$	F_d	B_{th}
>200 000 $\mathrm{A^2/mm^2/cm}$	30–60 $\mathrm{kN/m^2}$	≈0.30 T

2) Description of studied machine;
3) Analysis and Discussion;
4) Conclusion.

II. THE MACHINE UNDER STUDY

The machine under study is a modular HVDC permanent magnet synchronous machine (PMSM). Each segment is chosen as one base winding, which gives 32 segments for this machine. The geometrical parameters for this machine are presented in Table IV and V. The permanent magnet synchronous machine is designed using literature from Phyronen [12], Vaschetto [13], and Hanselmann [14].

A. Design Criteria

The primary literature for the design procedure used in this article is the one developed by Hanselmann. This design procedure assumes that the values presented in Table I are known. The design criteria/constraints can be seen in Table II. In addition, some criteria were used to make the design procedure less tedious. These criteria were added to the analytical design software to ensure that the generator could be air-cooled and have a good torque and tooth flux density. These criteria are presented in Table III. The design procedure was done iteratively until these constraints were fulfilled.

The fractional slot winding generator has non-overlapping concentrated windings. This fractional slot winding generator is a tooth wound with one winding concentrated around a single tooth. Since this is a single layer, the winding is wound around every other tooth. The design algorithm accurately determined the power and torque for this case. The only parameter that was changed in the numerical analysis was the number of turns (N_s). A comparison of the numerically and analytically calculated geometrical and electrical parameters is also presented in Table IV, V, and VI, respectively. The machine has full pitch, concentrated winding, and a slot per pole per phase (q) equal to 0.4. This q is chosen to avoid large torque ripples. The torque ripple mitigation is important to reduce its effect on the mechanical fasting holding the segments in place [15]. The cogging torque for this machine

TABLE IV
MACHINE STATOR PARAMETERS CALCULATED USING VASCHETTO AND HANSELMAN'S METHOD

Symbol	Analytical Value	Numerical Value
δ_m	0.01 m	0.01 m
A_{us}	1.0884×10^{-4} $\mathrm{m^2}$	1.0884×10^{-4} $\mathrm{m^2}$
D_o	10.2000 m	9.5718 m
D_{is}	9.8180 m	9003.6 mm
l_b	2.0178 m	2.0178 mm
Q_s	384	384
N_s	43	44
q	0.4	0.4
w_{tt}	0.0381 m	0.0381 m
w_{st}	0.0410 m	0.0410 m
J_s	1.3456 $\mathrm{A/mm^2}$	1.3456 $\mathrm{A/mm^2}$
h_{us}	0.1452 m	0.1452 m
k_w	0.9659	0.966

TABLE V
MACHINE ROTOR PARAMETERS CALCULATED USING VASCHETTO AND HANSELMAN'S METHOD

Symbol	Analytical Value	Numerical Value
h_m	0.0490 m	0.0490 m
τ_u	0.1606 rad	0.1606 rad
α	0.7	0.7
D_r	9.7000 m	9.7000 m
D_{ir}	9.6084 m	9.6084 m
N_p	320	320
τ_p	0.0964 rad	0.0964 rad

TABLE VI
ELECTRICAL PARAMETERS ANALYTICALLY AND NUMERICALLY DEDUCED

Symbol	Analytical Value	Numerical Value
$\hat{I}$	243.15 A	243.15 A
J_s	3 $\mathrm{A/m^2}$	3 $\mathrm{A/m^2}$
ω_e	167.55 rad/s	167.55 rad/s
t_{ins}	1.33 mm	1.33 mm
E_g	34.2130 kV	34.2130 kV
w_{seg}	10.0 mm	10.0 mm

TABLE VII
EXCITATION OF THE STATOR WINDINGS

Variable	No load	Full load
i_a	0	$\hat{I}\sin(2\pi ft + \Theta_q)$
i_b	0	$\hat{I}\sin(2\pi ft + +2\pi/3 + \Theta_q)$
i_c	0	$\hat{I}\sin(2\pi ft + 4\pi/3 + \Theta_q)$

is very low, which is also good in terms of design principles. This can be seen in Fig. 3. The electrical parameters for the generator can be seen in Table VI. The load angle (Θ_q) is calculated analytically and numerically. $\Theta_q = 2\pi f t_{max}$, where the time giving maximum numerical torque (t_{max}) is 0.02 s. The no and full load simulation are done using the assumptions presented in Table VII.

B. Matlab LiveLink

In the design procedure the machine Matlab live-link is utilize for a quick parameter updates. The design procedure is an iterative process and requires often many iterations.

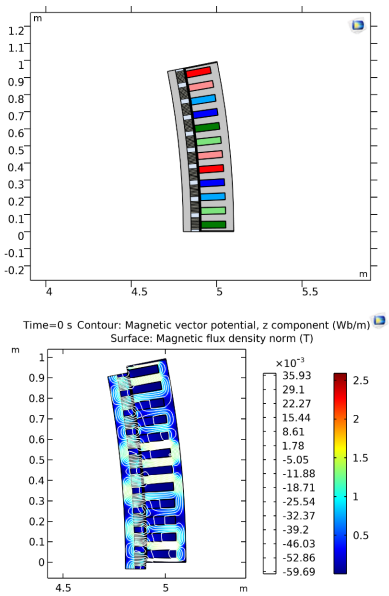

Fig. 1. Winding layout and flux distribution of the modular HVDC PMSM. Red is phase A, blue is phase B, and green is phase C. The darker shades indicate a positive phase, and the lighter shades indicate a negative phase.

To quickly update the analytically deduced geometrical and electrical parameters in the numerical software COMSOL, Matlab live-link for COMSOL is utilized. This significantly shortens the time procedure for the optimization of the design. The procedure is presented in Fig. 2. Matlab Livelink can also be utilized to see if the geometrical parameters are geometrically feasible. This can also be seen in Fig. 1.

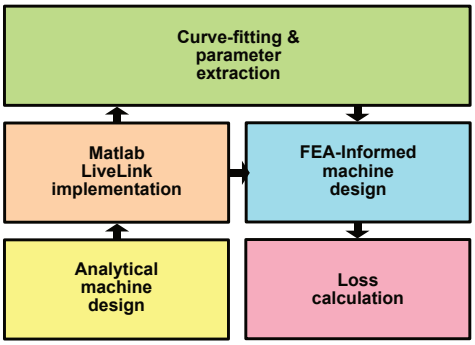

Fig. 2. Procedure for calculation of machine losses.

C. Loss Calculation

The loss where analytically deduced using Hanselmanns formula and numerically deduced using COMSOL. This can be seen in Table VIII. The material that was chosen for this generator is M250-50A [16]. The typical loss density datasheet, in addition to the frequency for different flux densities of the material, was used to determine the curve-fitting parameters of the material. The chosen method to determine the steel losses in the stator and rotor was CAL2 [17] and Zhang [18]. The curve-fitting parameters can be seen

TABLE VIII
ANALYTICALY DEDUCED IRON CORE AND COPPER LOSSES FOR GENERATOR G1

P_{fe}	P_{cu}
49.4949 kW	197.5778 kW
3.2997×10^{-3} pu	13.1719×10^{-3} pu

TABLE IX
LOSS COEFFICIENTS USED IN CAL2 AND ZHANG

Coefficient	CAL2	Zhang
k_{h0}	0.030 96	0.028 87
k_{h1}	−0.019 32	0
k_{h2}	−0.000 277 3	0
k_{h3}	0.004 144	0
k_{e0}	0.000 127 1	7.776×10^{-5}
k_{e1}	-7.22×10^{-5}	8.065×10^{-6}
k_{e2}	8.01×10^{-5}	3.795×10^{-7}
k_{e3}	1.95×10^{-5}	0

TABLE X
BERTOTTIS COEFFICIENTS

Loss coefficients	value
K_e	1.221×10^{-4}
K_a	3.472×10^{-5}
k_h	0.013 38
α	2.2

in Table IX. Regarding the material selection of the magnets, a neodymium (Nd) permanent magnet with a permeability of $1.2T$ was chosen for the generator (G1). The loss coefficients used in the Cal2 and Zhang method are presented in Table IX, where eqs. (1) and (2) were used in eq. (3) for the CAL2 method. The method is then compared with Bertotti [19] and Zhangs method [18]. The coeficients used in Bertottis method is presented in Table X.

$$K_h(\hat{B}) = K_{h0} + K_{h1}\hat{B}K_{h2}\hat{B}^2 + +K_{h3}\hat{B}^3 \tag{1}$$

$$K_e(\hat{B}) = K_{e0} + K_{h1}\hat{B}K_{e2}\hat{B}^2 + +K_{e3}\hat{B}^3 \tag{2}$$

$$p = K_h(f,\hat{B})\hat{B}^2 f + K_e(f,\hat{B})\hat{B}^2 f^2 \tag{3}$$

D. Numerical Analysis

The geometric parameters given in Table IV were used to create the machines in COMSOL Multi-Physics, where only the base winding of the generators is simulated in COMSOL. This is done to save computational time. The generator has a single layer where the phase layout can be seen in Fig. 1. The colors indicate the phase and the direction. The flux density distribution throughout the machine during full load can also be seen in Fig. 1. The three-phase voltage during full load can be seen in Fig. 3. The cogging torque and full load torque can also be seen in Fig. 3. The numerically calculated nominal torque corresponds well with the analytically estimated torque.

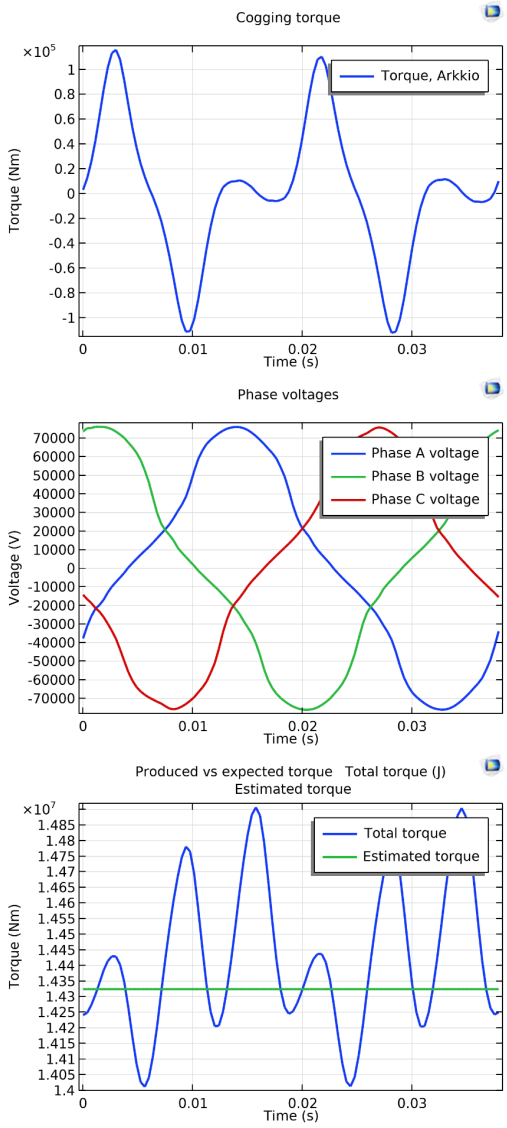

Fig. 3. Cogging torque, rated phase voltage, and total torque at full load.

TABLE XI
THE CORE LOSSES IN THE GENERATOR

Condition	Loss type	Bertotti	CAL2	Zhang
Full load	Hysteresis	56.085 kW	53.266 kW	87.570 kW
	Eddy current	11.252 kW	22.974 kW	10.220 kW
No load	Hysteresis	32.66 kW	36.137 kW	45.020 kW
	Eddy current	5.260 kW	6.415 kW	4.670 kW

III. Results and Discussion

A. Loss Analysis

1) Core Losses: Table XI presents the numerically calculated core losses. The numerical calculations show that the Bertottis method gives the lowest losses both for full load and no-load. The techniques for core loss calculation have similar eddy current losses but differ vastly for the hysteresis losses.

TABLE XII
MAGNET LOSSES

Condition	Segmentation	Value
Full load	Unsegmented	483.180 kW
	Segmented	53.613 kW
	Decrease	88.9 %
No load	Unsegmented	103.540 kW
	Segmented	25.026 kW
	Decrease	75.8 %

TABLE XIII
LOSS COMPONENTS AT FULL LOAD WITH SEGMENTED MAGNETS

Symbol	Bertotti	CAL2	Zhang
P_{cu}	240.590 kW	240.590 kW	240.590 kW
P_{fe}	67.337 kW	76.240 kW	97.790 kW
P_{pm}	53.613 kW	53.613 kW	53.613 kW
$P_{cu} + P_{fe} + P_{pm}$	361.540 kW	370.443 kW	391.993 kW
η_n	97.647 %	97.590 %	97.453 %

2) Magnet Losses and Segmentation: The numerically calculated magnet losses are presented in Table XII. The numerical calculations show the percentage decrease in losses between the segmented and unsegmented magnets. The considerable difference in losses made the design choice easy in terms of segmentation. The table presents the magnet losses for both full and no load.

3) Total Losses: Table XIII presents the numerically calculated total losses. The numerical calculations show that the Bertottis method gives the lowest total losses due to the low core losses. I have neglected the stray load losses, due to the difficulty in estimating such losses. They often decrease the efficiency in a magnitude of several percent [14]. The table presents the efficiency of the machine for the different techniques. The efficiency of the machine is calculated using the following formula.

$$\eta_n = \frac{P_{nom}}{P_{nom} + P_{fe} + P_{pm} + P_{cu}} \tag{4}$$

4) Impact of Different Segment Airgap Lengths: The core losses in the generator for different segment airgap lengths are presented in Table XIV.

TABLE XIV
GENERATOR CORE LOSSES FOR DIFFERENT SEGMENT AIRGAP LENGTHS AT FULL LOAD CONDITION

Segment airgap	Bertotti	CAL2	Zhang
0 mm	63.832 kW	76.215 kW	83.460 kW
10 mm	67.337 kW	76.240 kW	97.790 kW
	+5.344 %	+0.033 %	+15.812 %
20 mm	66.792 kW	77.522 kW	98.380 kW
	+4.532 %	+1.700 %	+16.410 %
30 mm	65.583 kW	74.707 kW	97.870 kW
	+2.706 %	+1.998 %	+15.894 %

B. Discussion of Results

1) Core Losses: Core losses are difficult to estimate and can differ quite significantly. This is because of how these losses

are simulated and the assumptions in the different methods. E.g in this case Bertotti's and CAL2 coefficient is fitted for three frequencies. These frequencies are $50\,\mathrm{Hz}$, $100\,\mathrm{Hz}$ and $200\,\mathrm{Hz}$. While Zhangs coefficients are fitted for the frequencies $50\,\mathrm{Hz}$, $100\,\mathrm{Hz}$, $200\,\mathrm{Hz}$, $400\,\mathrm{Hz}$ and $1000\,\mathrm{Hz}$. Different fitting causes difference in coefficients, which again causes Bertotti and CAL2 to differ from Zhang. Another reason for the relative big difference in core losses is because of the domain the simulation are made in. Bertotti and CAL2 are simulated in time domain, while Zhangs method is simulated in frequency domain.

2) Magnet Losses and Segmentation: The segmentation of the magnets makes it so that one has a significant loss reduction because one has a smaller current density surface, which reduces the circulating currents [20].

3) Total Losses: Table XIII shows that the copper losses are the most predominant because of the high number of turns and copper fill factor used to get the required voltage.

The generator has a relatively low frequency ($f = 26.67\,\mathrm{Hz}$), which gives relatively low core losses because the core losses depend on the machine's frequency and flux density [21].

The magnet is segmented, which significantly reduces the losses.which is because the segmentation minimizes the area of the circulating current, which substantially reduces the eddy current losses [20].

4) Impact of Different Segment Airgap Lengths: Table XIV shows specific segment airgap lengths, default segment length (highlighted in cyan), non modularity (highlighted in marron) and the precentage difference in core losses caused by modularity. I.e. non-modular gen. loss is compared with modular gen. loss for different segment airgap lengths.

The table shows a significant difference. This is because the flux gets trapped inside each segment (i.e., a higher concentration of flux inside each segment, particularly at the segement ends), which means that no flux is leaking between the segments, which again gives higher core losses in comparison to a non-modular generator. For a non-modular generator, the flux would be more evenly distributed, giving lesser core losses.

IV. Conclusion

This paper presents the concept of a modular HVDC generator and explains how this generator can reduce the number of conversion steps for offshore wind, where the idea is validated numerically using FEA. Three different methods are used to calculate the machine's core losses. We also present total losses, and efficiency, in addition the core losses for other segment air gaps. The main highlights include the following:

1) Numerical validation of the modular HVDC generator;
2) A comparison of different iron loss calculations, demonstrating the volatility of iron loss estimation.
3) Magnet segmentation highly reduces the losses.
4) For a certain segment airgap length, the flux does not leak between the segments, causing the core losses to be somewhat constant and higher compared to the non-modular generator.

Future work will possibly focus on different loading conditions and thermal conditions for this type of machine. This will be done through co-simulation, where the time harmonics of the converters will be included.

References

[1] M. Borgersen, "Custom design and analysis of modular high voltage dc generator," 2019.

[2] I. Dincer, "High-power wind energy conversion systems: State-of-the-art and emerging technologies," vol. 103, no. 5, pp. 740–788, 2015.

[3] T. Ackermann, *Wind Power in Power Systems*, 1st ed. Chichester: Wiley, 2005, iSBN : 0470855088.

[4] "Welcome to the Global Wind Atlas," https://globalwindatlas.info/, 2021, [Online; accessed 11-November-2021].

[5] O. Anaya-Lara, *Offshore Wind Energy Generation: Control, Protection, and Integration to Electrical Systems*, 1st ed. Chichester: Wiley, 2014, iSBN : 1-118-70153-4.

[6] I. Dincer, "Reneweable energy and sustainable development: A crucial review," vol. 4, no. 2, pp. 157–175, 2000.

[7] T. C. Trust, "The Offshore Wind Accelerator," https://prod-drupal-files.storage.googleapis.com/documents/resource/public/DC-Array-summary-2021.pdf, 2021, [Online; accessed 12-November-2021].

[8] M. Pape and M. Kazerani, "An offshore wind farm with dc collection system featuring differential power processing," *IEEE Trans. Energy Convers.*, vol. 35, no. 1, pp. 222–236, 2020.

[9] F. An, B. Zhao, B. Cui, and R. Bai, "Multi-functional dc collector for future all-dc offshore wind power system: Concept, scheme, and implement," *IEEE Trans. Ind. Electron.*, vol. 69, no. 8, pp. 8134–8145, 2022.

[10] Y. Fu, Y. Liu, L.-l. Huang, F. Ying, and F. Li, "Collection system topology for deep-sea offshore wind farms considering wind characteristics," *IEEE Trans. Energy Convers.*, vol. 37, no. 1, pp. 631–642, 2022.

[11] GWEC, "Global wind report 2021." [Online]. Available: https://gwec.net/wp-content/uploads/2021/03/GWEC-Global-Wind-Report-2021.pdf

[12] J. Pyrhonen, V. Hrabovcova, and T. Jokinen, *Design of Rotating Electrical Machines*, 1st ed. New York: Wiley, 2009.

[13] S. Vaschetto, A. Tenconi, and G. Bramerdorfer, "Sizing procedure of surface mounted PM machines for fast analytical evaluations," in *Proc. IEEE Int. Electr. Mach. Drives Conf. (IEMDC)*, 2017, pp. 1–8.

[14] D. Hanselmann, *Brushless Permanent Magnet Motor Design*, 2nd ed. Maine: Wiley, 2003.

[15] G. Dajaku and D. Gerling, "A novel 12-teeth/10-poles pm machine with flux barriers in stator yoke," in *Proc. Int. Conf. Electr. Mach. (ICEM)*, 2012, pp. 36–40.

[16] R. Mellerud, "Analysis of losses and radial vibration in a pm synchronous machine with physical modularity," 2021.

[17] D. Ionel, M. Popescu, M. McGilp, T. Miller, S. Dellinger, and R. Heideman, "Computation of core losses in electrical machines using improved models for laminated steel," *IEEE transactions on industry applications*, vol. 43, no. 6, pp. 1554–1564, 2007.

[18] Z. Zhang, A. Nysveen, R. Nilssen, B. J. Fagermyr, A. Chen, and H. Ehya, "Material characterization and stator core loss computation of synchronous generators with stacking force accounted," in *Proc. Int. Conf. Electr. Mach. (ICEM)*, 2022, pp. 2169–2175.

[19] G. Bertotti, "General properties of power losses in soft ferromagnetic materials," *IEEE Trans. Magn.*, vol. 24, no. 1, pp. 621–630, 1988.

[20] D. Ishak, Z. Zhu, and D. Howe, "Eddy-current loss in the rotor magnets of permanent-magnet brushless machines having a fractional number of slots per pole," *IEEE Trans. Magn.*, vol. 41, no. 9, pp. 2462–2469, 2005.

[21] P. A. Hargreaves, B. C. Mecrow, and R. Hall, "Calculation of iron loss in electrical generators using finite-element analysis," *IEEE Trans. Ind. Appl.*, vol. 48, no. 5, pp. 1460–1466, 2012.